ELSEVIER

Journal of Power Sources 114 (2003) 253–263

JOURNAL OF POWER SOURCES

www.elsevier.com/locate/jpowsour

Electrochemical investigations on electrostatic spray deposited $LiMn_2O_4$ films

Dong Shu[a,*], Kyung Yoon Chung[a], Won Il Cho[b], Kwang-Bum Kim[a]

[a]*Department of Metallurgical Engineering, Yonsei University, 134 Shinchon-dong, Seodaemun-gu, Seoul 120 749, South Korea*
[b]*Eco & Nano Research Center, Korea Institute of Science and Technology, P.O. Box 131, Cheongryang, Seoul 136 791, South Korea*

Received 17 July 2002; accepted 21 October 2002

Abstract

$LiMn_2O_4$ films have been prepared using an electrostatic spray deposition (ESD) technique at 400 °C. The deposited films are investigated by means of X-ray diffraction (XRD), scanning electron microscopy (SEM), electrochemical quartz crystal microbalance (EQCM), cyclic voltammetry (CV), galvanostatic charge–discharge, and electrochemical impedance spectroscopy (EIS). Analysis of $LiMn_2O_4$ films using XRD and SEM indicates the formation of a $LiMn_2O_4$ single spinel phase with a uniform and dense film. On the other hand, electrochemical investigation in a non-aqueous electrolyte (1 M $LiClO_4$ + EC + DEC) suggests the formation of surface film after the initial dissolution of Li_2CO_3 layer, the mass of surface film has been calculated from the resonant frequency curve and is about 1.2% of entire $LiMn_2O_4$ film. The results of CV, EQCM and EIS studies are discussed in terms of changes in surface electrochemical properties during the lithium insertion–extraction process.

Keywords: $LiMn_2O_4$; Electrostatic spray deposition; Electrochemical quartz crystal microbalance; Impedance spectroscopy; Lithium-ion battery

1. Introduction

Lithium transition metal oxides have been the focus of attention since the first commercialization of Li-ion batteries by Sony Energetics in 1990 [1]. Although $LiCoO_2$ is the cathode material that is widely used in Li-ion batteries, $LiNiO_2$ and $LiMn_2O_4$ have been suggested as possible alternatives. Among these cathode materials, $LiMn_2O_4$ is very attractive in terms of cost, toxicity and ease of preparation, but still suffers from the disadvantages of capacity fading and formation of a surface film [2].

Tarascon and co-workers [3] reported the presence of a surface film on $LiMn_2O_4$ particles after storage in electrolyte at elevated temperature. It was also suggested that this electrochemically inactive film is responsible for initial capacity loss. Moreover, TGA and FTIR studies by these authors showed the inorganic nature of these films and the composition was found of vary with storage time. Aurbach et al. [4] also investigated the surface phenomena of $LiMn_2O_4$ using different spectroscopic techniques (XPS, EDAX, FTIR, etc.) and concluded that the pristine $LiMn_2O_4$ is masked by a surface film which is mainly composed of Li_2CO_3. Further, it was suggested that during the subsequent electrochemical process, the Li_2CO_3 film dissolved and was replaced by solution-related surface species and salt-reduction products that influenced the impedance behavior and kinetics of the electrode. Since ex situ techniques were employed by these authors, the exact potential and time range at which the surface film occurred could not be determined precisely.

In view of the above, it is worthwhile to explore the possibility of employing more sensitive in situ techniques for understanding the nature of the surface films which surround the $LiMn_2O_4$ particles. The electrochemical quartz crystal microbalance (EQCM) is an in situ mass-sensitive detector based on the measurement of resonant frequency changes induced by mass or viscosity changes of a film attached to a quartz crystal substrate during electrochemical measurements [5]. This technique is particularly attractive for lithium-ion battery research because an intercalation reaction of lithium ions in active materials is accompanied by a mass change [6–15], it may distinguish the intercalation reactions of lithium ions in an electrode from chemical and electrochemical reactions. The formation of surface film results in a mass change of the electrode, which can be detected by in situ EQCM techniques.

* Corresponding author. Present address: Chemistry Department, Zhaoqing University, Guangdong Province 526061, PR China.
Tel.: +86-758-2716452.
E-mail address: shudong66@hotmail.com (D. Shu).

0378-7753/02/$ – see front matter
PII: S0378-7753(02)00602-X

The success of the EQCM-based studies lies in the preparation of thin films on the EQCM electrode. The thin films can be realized by using techniques such as the spin-coating method [8,14,15], the sol–gel method [12], thermal vacuum evaporation [10], the electrochemical Au-co-deposition method [16], the radio frequency sputter deposition method [9], etc. Preparation of thin films using an electrostatic spray deposition (ESD) technique is, however, more easy and involves less time and sophistication. The ESD technique has recently gained importance in Li-ion battery development given the successful preparation of thin films of $LiCoO_2$, $LiNiO_2$, and $LiMn_2O_4$ [13,17–19]. The main advantages associated with the ESD technique are the elimination of co-additives in the cathode electrodes, e.g. carbon black and PVDF, and the fact that the films can be obtained at low temperature, i.e. 400 °C for materials like $LiMn_2O_4$. This low temperature is very important as far as EQCM are concerned because a quartz crystal undergoes α–β phase transition at 537 °C.

In this paper, the preparation of spinel $LiMn_2O_4$ film by the ESD technique is reported. The film has been electrochemically investigated using cyclic voltammetry (CV), charge–discharge, EQCM and electrochemical impedance spectroscopy (EIS) techniques.

2. Experimental

Lithium acetate ($CH_3COOLi{\cdot}2H_2O$), manganese nitrate ($Mn(NO_3)_2{\cdot}4H_2O$) and ethanol (EtOH) (Aldrich, AR) were used as received without further purification for preparing the precursor solution for $LiMn_2O_4$ ESD thin films. Details of the ESD set-up and working principle are described elsewhere [18–20]. In the present study, a precursor solution consisting of 25 mM CH_3COOLi + 50 mM $Mn(NO_3)_2$ in EtOH was pumped at 2 ml h^{-1} through a stainless-steel nozzle. The $LiMn_2O_4$ film was deposited on to a commercially available Pt-coated AT-cut quartz crystal electrode (resonance frequency: 9 MHz, 0.2 cm^2 geometric electrode area, Seiko EG&G). The substrate temperature was maintained at 400 °C during the deposition and then the deposited film was annealed further for 1 h at 400 °C in an air oven. The mass change of the deposited electrode material was calculated using the Sauerbrey equation [5]. A scanning electron microscope (SEM, Hitachi S2700) was used for examining the surface morphology and determining the thickness of the film.

EQCM measurements were carried out using the basic instrument supplied by EG&G (QCA917). A potentiostat (EG&G, M273) was used in conjunction with the EQCM instrument. Electrochemical impedance spectroscopy measurements were performed with a Solartron 1287 electrochemical interface and 1260 impedance/gain-phase analyzer driven by the Zplot software in the frequency range 10^{-2} to 10^5 Hz.

All electrochemical measurements were carried out using a three-electrode cell which was assembled under an argon atmosphere in a glove box. The studies were carried out with the ESD $LiMn_2O_4$ film as working electrode in non-aqueous electrolyte (1 M $LiClO_4$ + EC + DEC) using lithium foil as reference and counter electrodes (EC: ethylene carbonate; DEC: diethyl carbonate).

3. Results and discussion

The XRD pattern of the $LiMn_2O_4$ thin film obtained using the ESD technique at 400 °C on a Pt–Si wafer substrate is presented in Fig. 1. In order to minimize interference from the diffraction peaks of the substrate, near grazing angle

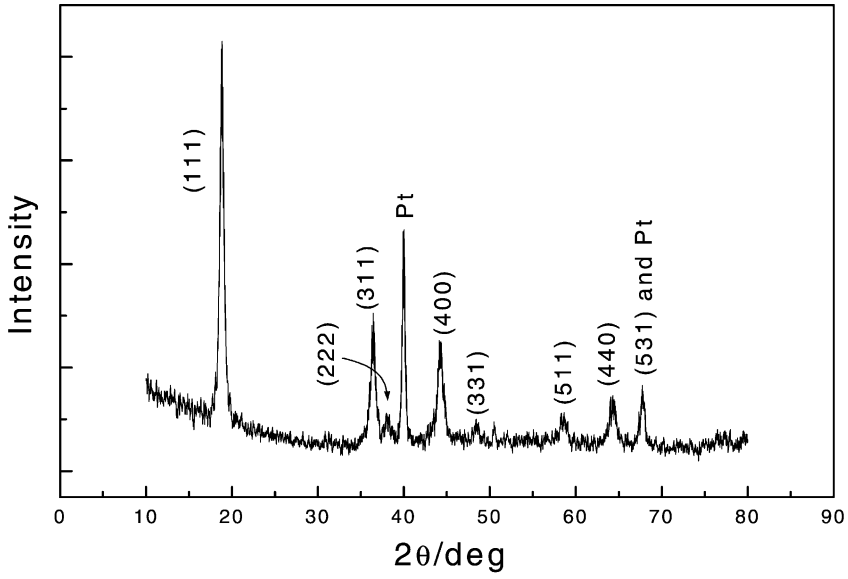

Fig. 1. XRD spectra of $LiMn_2O_4$ film prepared on Pt–Si substrate by ESD at 400 °C.

scans were made in which the angle of the incident radiation with respect to the plane of the substrate was fixed at 5° while the detector with a parallel-beam thin film attachment placed in front of it was moved through the 2θ angle. It can be seen clearly that all the *h k l* peaks can be indexed to the spinel structure of $LiMn_2O_4$ and represent the space group, *Fd3m*. The two peaks of the substrate due to platinum are also indicated in Fig. 1. Thus, the position of the Li and Mn ions can be assigned the 8a tetrahedral and 16d octahedral sites, respectively [21]. Further, it is interesting to note that the $LiMn_2O_4$ was synthesized at low temperature (400 °C) in spite of the fact that conventionally $LiMn_2O_4$ is synthesized at higher temperature (700–800 °C) and requires a long process time (24–48 h) [22,23].

Scanning electron micrographs of the cross-section of the film deposited on the substrate and the surface morphology of $LiMn_2O_4$ are shown in Fig. 2. It is clear that the film is uniform, dense, compact and adherent to the substrate, which indicates its applicability for EQCM investigations. Further, the film was obtained within 4–5 min using the ESD technique. The optimum thickness of the film was found to be 0.45 μm. It should be emphasized here that too thin a film affects the precision of electrochemical measurements whereas too thick a film limits the applicability of EQCM.

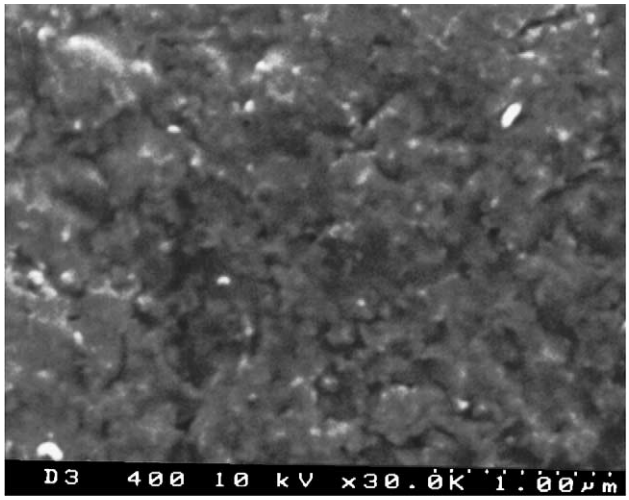

(a)

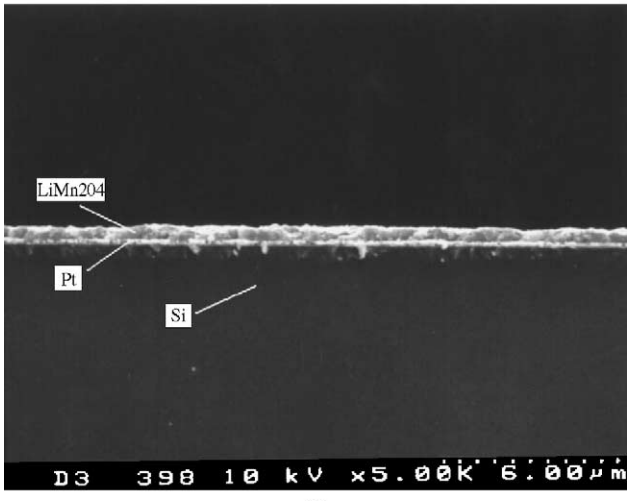

(b)

Fig. 2. (a) Scanning electron micrograph of $LiMn_2O_4$ film prepared on Pt–Si substrate by ESD at 400 °C. (b) Scanning electron micrograph showing cross-section of $LiMn_2O_4$ film prepared on Pt–Si substrate by ESD at 400 °C.

A cyclic voltammogram and the frequency response of the $LiMn_2O_4$ ESD film in the second cycle are shown in Fig. 3a and b, respectively. The experiment was performed in $LiClO_4$ + EC + DEC electrolyte at 30 °C. A pair of oxidation and reduction peaks appear around 4.0 and 4.15 V in the CV curve, which is in agreement with the results reported by several other researchers [24,25]. These two peaks are normally assigned to the extraction–insertion of Li ions from–into the tetrahedra sites [26]. Lim et al. [16] assigned the peaks at low potential to the extraction–insertion of Li ions in a one-phase structure, and those at higher potential to insertion–extraction of Li^+ ions between $LiMn_2O_4$ and λ-MnO_2. The variation in the resonant frequency of the quartz crystal electrode was monitored simultaneously during the CV scan. The insertion–extraction of Li^+ ions into–from $LiMn_2O_4$ film has a direct bearing on the frequency of the EQCM, i.e. the frequency increase on extraction of Li^+ ions indicates a decrease in the mass of the electrode, and vice versa. Further, the frequency variation shows two steps related to two peaks in the cyclic voltammogram.

The variation of resonant frequency and the theoretical values of frequency during cyclic voltammetry are shown in Fig. 3b. The theoretical values were calculated from the CV data assuming one electron transfer per equivalent of Li. The change in frequency is larger than that predicted theoretically and is almost reversible. Because of the decomposition of electrolyte, however, the theoretical curve indicates that the charge in frequency in the oxidation process is larger than in the reduction process. The mass change per mole of electron (m.p.e.) values are 15 and 26 in the potential range 3.6–4.3 V during oxidation (extraction) and reduction (insertion), respectively. The m.p.e. values are higher in comparison with the molecular weight of Li (6.94 g mol^{-1}). The m.p.e. values for every 20 mV potential scan in the range 3.9–4.3 V are higher than the molecular weight of Li and can be ascribed to the side reactions or co-intercalation of solvents (Fig. 3c). Further, an increase in potential results in a decrease in m.p.e. values due to the decomposition of solvent on the electrode surface at high anodic potentials.

It should be noted that a similar shape of cyclic voltammogram (Fig. 4a) obtained in the second cycles but the cyclic voltammassogram, i.e. resonant frequency changes, (Fig. 4b) is different. Normally, when Li^+ ions are extracted from the $LiMn_2O_4$ film, the decrease in mass is accompanied by an increase in frequency, but the frequency decreases abnormally with increase in the mass of electrode at potentials in the range 4.17–4.4 V. This phenomenon has not been previously reported. Then frequency curves of the first cycle superimposed on the second cycle are given in Fig. 5.

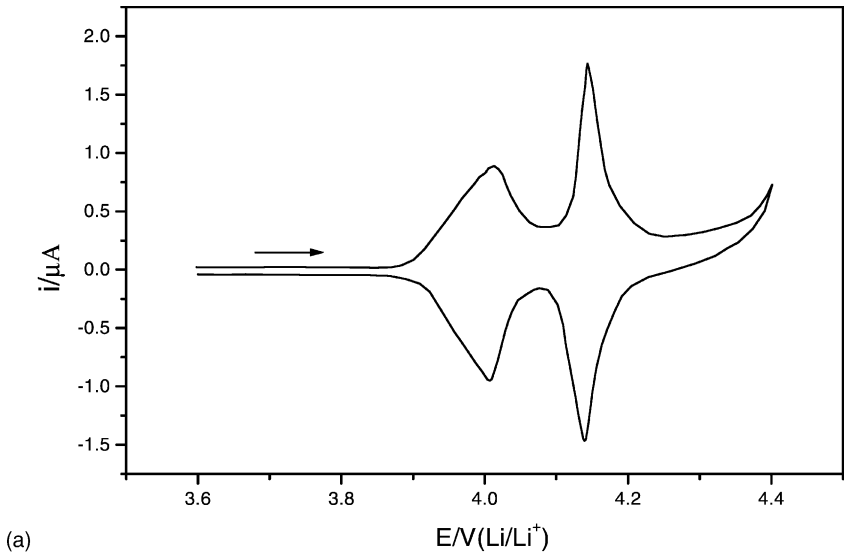

(a)

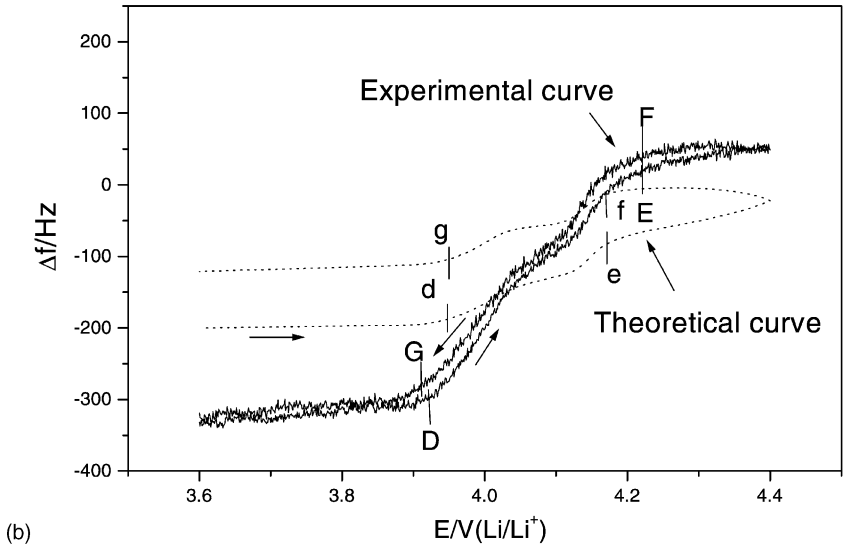

(b)

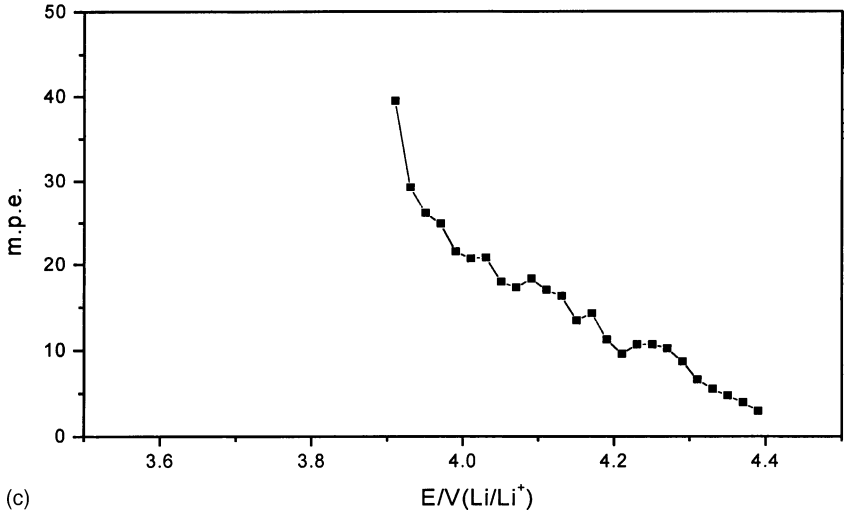

(c)

Fig. 3. (a) Cyclic voltammograms of a $LiMn_2O_4$ ESD film at 0.1 mV s^{-1} (second cycle). (b) Variation of resonant frequency during CV(solid curve) and theoretical values (dashed curve). (c) The m.p.e. value for every 20 mV anodic potential scan. Experiments conducted in 1 M $LiClO_4$ + EC + DEC at 30 °C. Mass of $LiMn_2O_4$ film is about 11.9 μg.

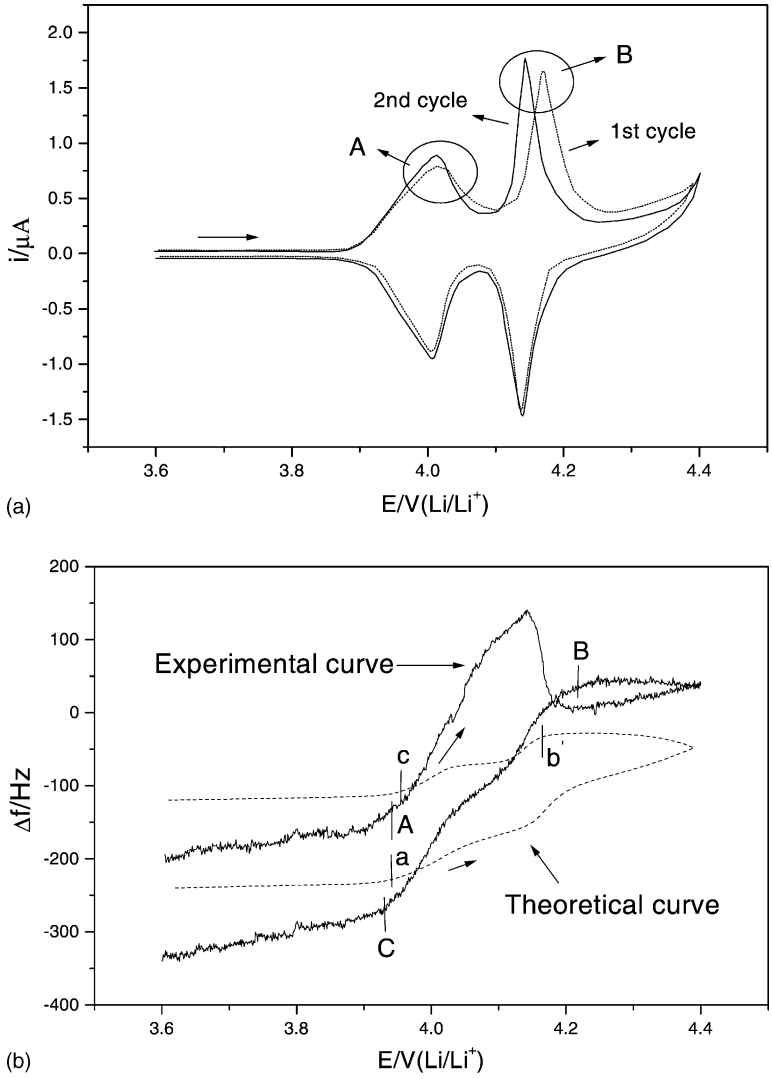

Fig. 4. (a) Cyclic voltammograms of $LiMn_2O_4$ ESD film at 0.1 mV s^{-1} (first and second cycle). (b) Variation of resonant frequency during CV (solid curve) and theoretical values (dashed curve) on first cycle. Experiments conducted in 1 M $LiClO_4$ + EC + DEC at 30 °C.

The curves overlap in the voltage range 3.6–4.04 V, but excess frequency appears in the first oxidation cycle at higher potentials (4.04–4.14 V) and an abnormal frequency decrease at 4.17–4.2 V. Pristine $LiMn_2O_4$ is found to be associated with a surface film of Li_2CO_3. Aurbach et al. [4] have suggested the dissolution of this film followed by the simultaneous formation of a new film due to the interaction of the active mass and the electrolyte during the subsequent electrochemical process. Thus, it is concluded that the excess frequency increase is due to the dissolution of a Li_2CO_3 layer on pristine $LiMn_2O_4$, whereas the abnormal frequency decrease is associated with the formation of a new surface film. Further, the new surface film strongly effects the nature of the Li intercalation process, e.g. solid-state diffusion and accumulation, migration of Li^+ ions though the surface film, and charge transfer of the Li^+.

An irreversible frequency change is observed in the first cycle and a reversible change in the second cycle (see Fig. 5). It is suggested that the former is mainly due to formation of surface film. Therefore, the mass of the surface film can be calculated from the resonant frequency curve and is about 0.14 μg and 1.2% of the entire $LiMn_2O_4$ film.

Some differences in the cyclic voltammogram for the first and second oxidation cycles are also noticed in Fig. 4a. For example, shape of the peaks at lower oxidation potentials (∼4 V) is different (region A) and the high voltage oxidation peak (∼4.15 V) shifts to a lower potential after the first cycle (region B). Further, it is interesting to note that the pairs of reduction peaks are almost symmetrical in both the cycles. These results imply some difference between the first oxidation cycle and the subsequent process. It is likely the formation of new surface film on the first oxidation cycle is responsible for this behavior.

In order to substantiate the above observations, the changes in frequency response during a typical constant-current charge–discharge process has been monitored (Fig. 6a)

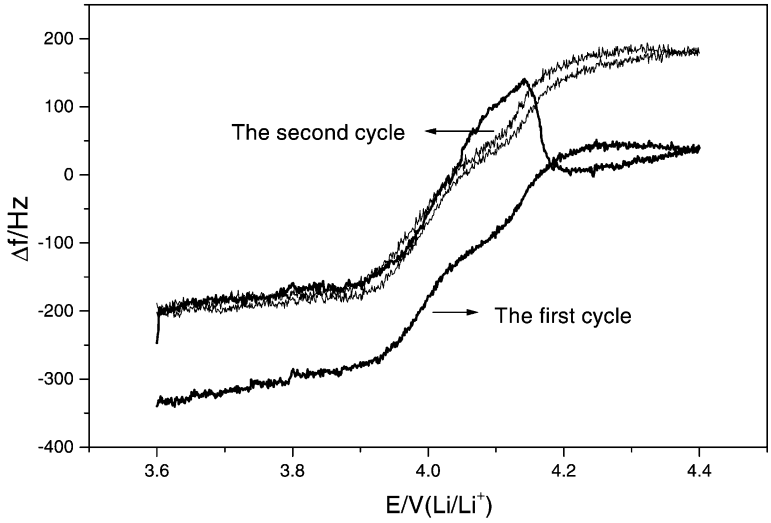

Fig. 5. Superimposed figure of frequency resonant curves on first and second CV cycles.

using the same electrolyte ($LiClO_4$ + EC + DEC). Similar behavior is observed, i.e. the frequency increases rapidly up to 4.16 V, but thereafter decreases abnormally. The frequency decreases are due to Li^+ ion insertion in the reduction process. Thus, it is confirmed that the rapid frequency increase is due to the extraction of Li^+ ions and the dissolution of the Li_2CO_3 layer, while the abnormal frequency response is due to the formation of the surface film. Furthermore, the experimental curve is steeper than the theoretical counterpart. These results support the observation made in CV studies.

It can be recalled from Fig. 4b that during the first oxidation cycle, the extraction of Li^+ ions from the $LiMn_2O_4$ film leads to a rapid increase in frequency at potentials up to 3.94 V (marked (A)) which agrees with the theoretical curve (marked (a)) and indicates that the frequency changes and current (related to theoretical frequency curve) are synchronous. During the reduction process, i.e. insertion of Li^+ ions into the $LiMn_2O_4$ film, the frequency begins to decrease sharply, the potentials are about 4.22 V (B) and 4.16 V (b′) in the experimental and theoretical curves, respectively. Further, the frequency change is ahead of current. Scanning the electrode to lower potentials leads to a slow decrease in frequency. The potentials are now 3.92 V (C) and 3.95 V (c) in the experimental and theoretical curves, respectively. This indicates that the current and frequency are not synchronous. Moreover, the second CV cycle (Fig. 3b) shows the expected behavior, i.e. current and frequency are not synchronous during both oxidation and reduction process. Hence, when current appears (d and f), the frequency change (D and F) is ahead of the current, while the current is ahead of the frequency (E and G) when it disappears (e and g). Thus, it can be concluded that the surface property of the electrode changes after the formation of the new surface film during the first oxidation process. Probably, some non-faradic processes appear when Li^+ ions are inserted into or extracted from a $LiMn_2O_4$ film due to chemical reaction or co-intercalation of solvents.

Electrochemical impedance spectroscopy is one of the most powerful techniques for investigating the nature of the surface of an electrode during an electrochemical process. As described, EQCM and cycling results have been related to surface film dissolution and formation. Hence, it is worthwhile to study the impedance behavior of the electrodes at various depths of charge–discharge.

The impedance spectra of ESD $LiMn_2O_4$ film measured at different potentials from 3.6 to 4.3 V are shown in Fig. 7a–e for several cycles with a relaxation time (1 h) after each impedance measurement. A semicircle in the high-frequency region can be assigned to the surface resistance (R_S) and the capacitance (C_S); it is related to Li^+ ion migration through the surface layer. A further medium-frequency semicircle is observed and is attributed to charge transfer at the interface between the surface and the active mass (R_{CT}), coupled with the double layer capacitance(C_{DL}). A straight line, characteristic of a Warburge-type element which reflects the solid-state diffusion of Li^+ ions into the active mass, is observed at low frequency. Further, at very low frequencies, the Z'' versus Z' plots become steeper, which indicates to the capacitance behavior and relates intercalation capacity of the electrodes and is strongly potential dependent.

It is interesting to note that the impedance spectra in the first oxidation cycle is different from other processes (Fig. 7a–c), but become similar at potentials higher than 4.2 V (Fig. 7d and e). The surface layer (R_S) and charge transfer (R_{CT}) resistance calculated from the diameter of the high- and medium-frequency semicircles in the Nyquist plots are shown in Figs. 8 and 9, respectively. It can be seen in Fig. 8 that the R_S values are the same at low potential ($E \leq 4.0$ V) but lower values of R_S appear above 4.1 V and these can be ascribed to decomposition of electrolyte.

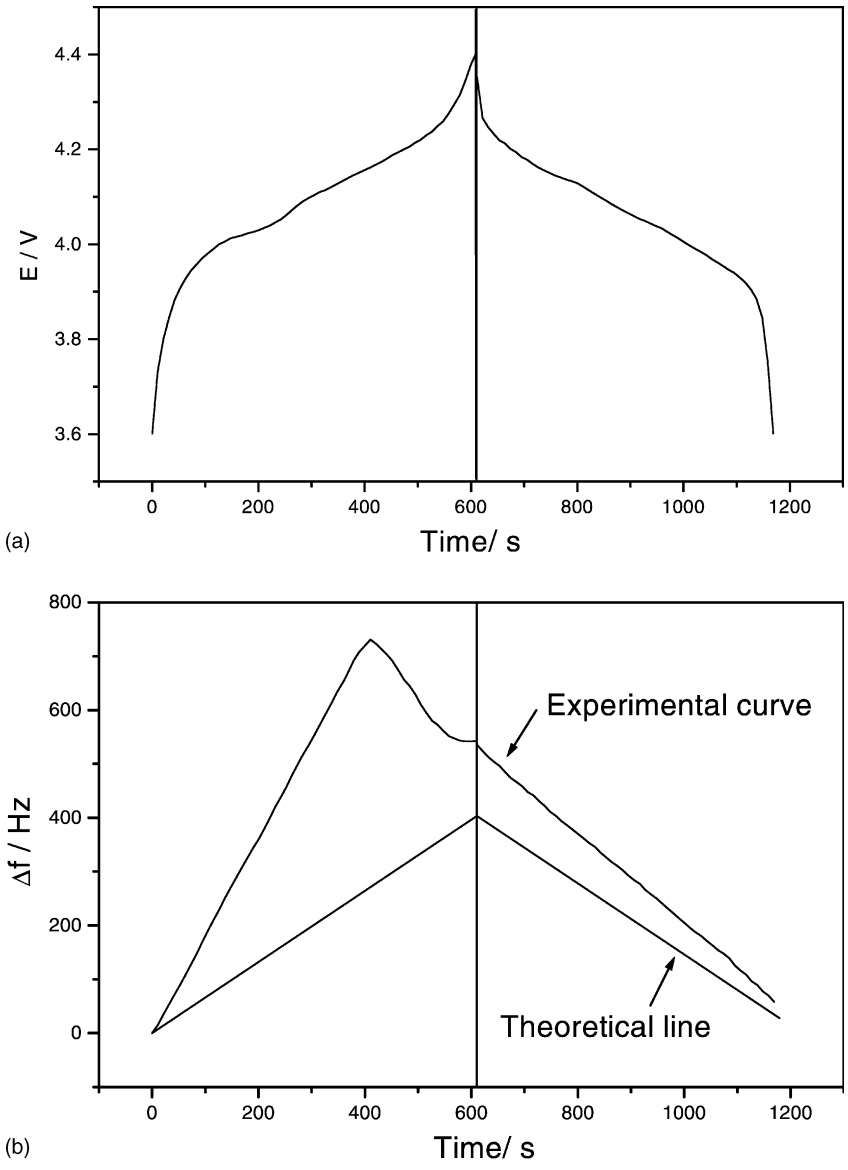

Fig. 6. (a) Charge–discharge curve of $LiMn_2O_4$ ESD film at 50 μ A cm^{-2}. (b) Variation of resonant frequency during charge–discharge cycle and theoretical straight line assuming one electron transfer equivalent of lithium. Experiment conducted in 1 M $LiClO_4$ + EC + DEC at 35 °C. Mass of $LiMn_2O_4$ film is about 8.4 μg.

At certain potentials, however, the R_S values in the first oxidation cycle are smaller than those in subsequent cycles and the amplitude is maintained after the first oxidation cycle. Similar behavior is observed in EQCM measurements and thereby confirm the formation of a surface film after the first oxidation cycle.

High R_{CT} values appear at potentials below 3.9 V and above 4.2 V, see Fig. 9, as found by other researchers [4,27,28]. This phenomenon is consistent with the observations for cyclic voltammograms where the current is almost zero at these potentials, the intercalation–deintercalation of a small quantity of Li^+ ion results in high R_{CT} values in these regions. Nishizawa et al. [29] also found some qualitative correlation between a drop in R_{CT} at high potentials and a drop in electronic conductivity of the spinel obtained by in situ conductivity measurements on thin films of $LiMn_2O_4$. In the potential range 3.7–4.1 V, the R_{CT} value in the first oxidation cycle is clearly smaller than that in subsequent cycles, where the values are the same after the first oxidation cycle in different cycles at the same potential. At 4.2 V, the R_{CT} value for the first oxidation cycle is closer to those for other reduction processes and can be assigned due to the formation of a surface film. These results confirm the EQCM results and is due to the changing surface properties as well as the change-transfer resistance which leads to an enhancement of surface resistance after the formation of a new surface film.

The formation of a surface film should affect the diffusion of Li^+ ions in the $LiMn_2O_4$ ESD film. Thus, the diffusion coefficients of Li^+ ions has been evaluated by potential step

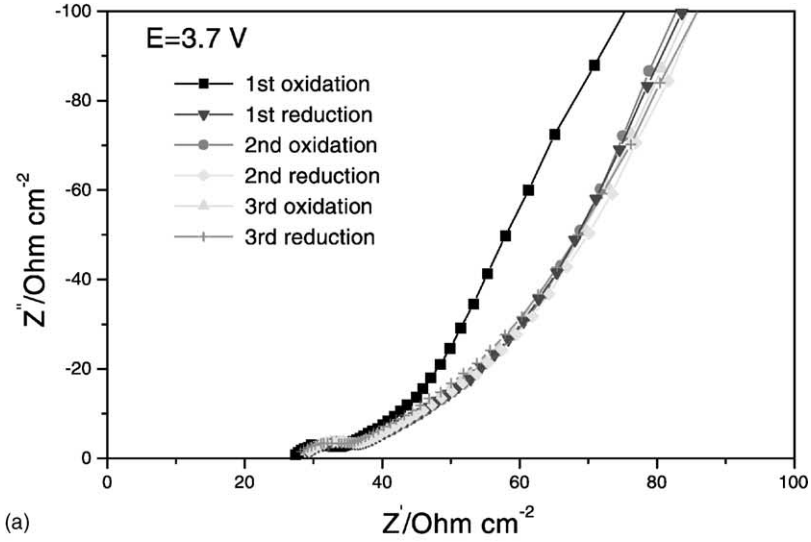

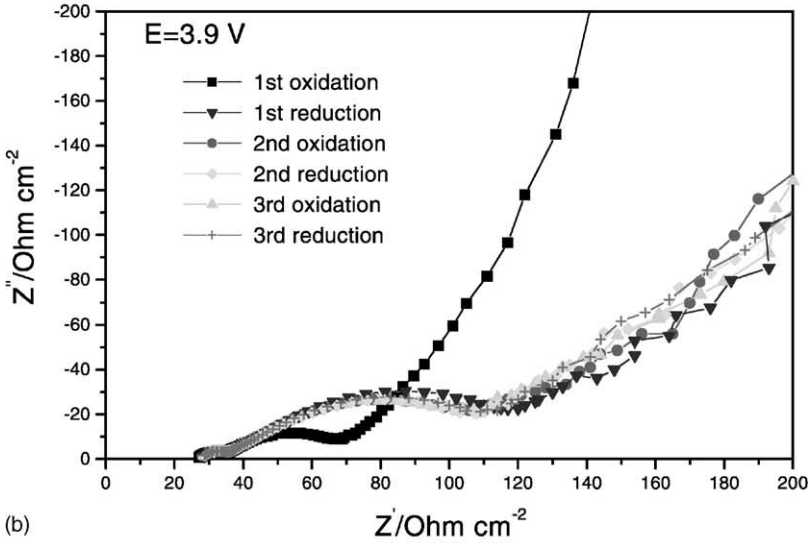

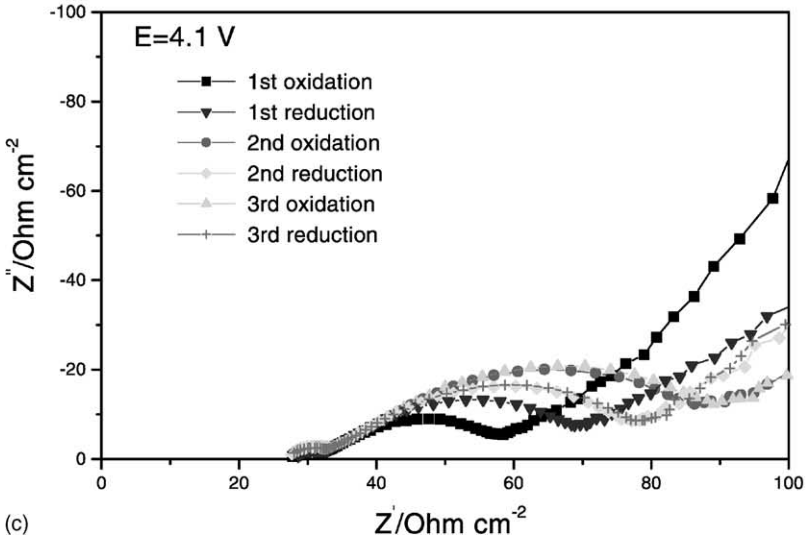

Fig. 7. Nyquist plots measured from $LiMn_2O_4$ film electrode at different potential and cycle number, as indicated.

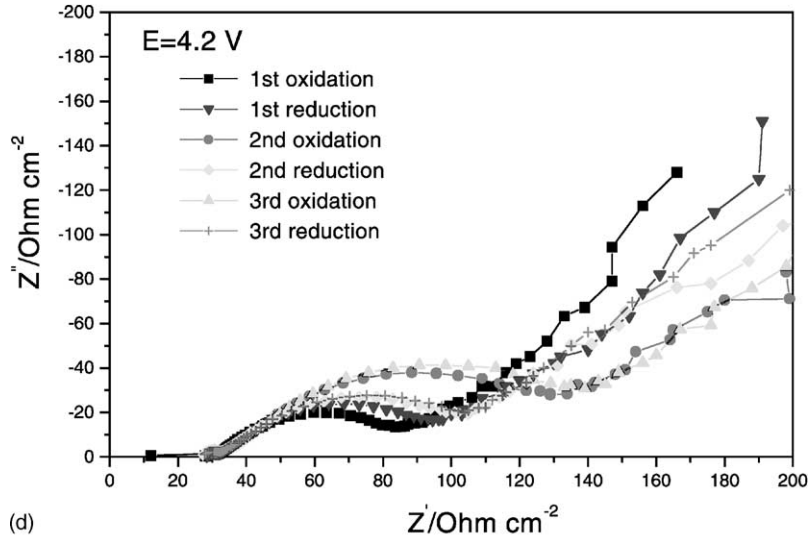

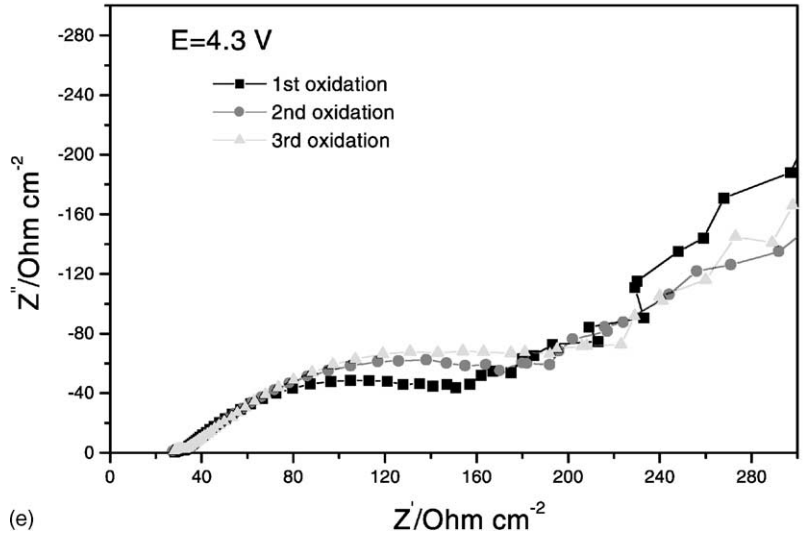

Fig. 7. (*Continued*).

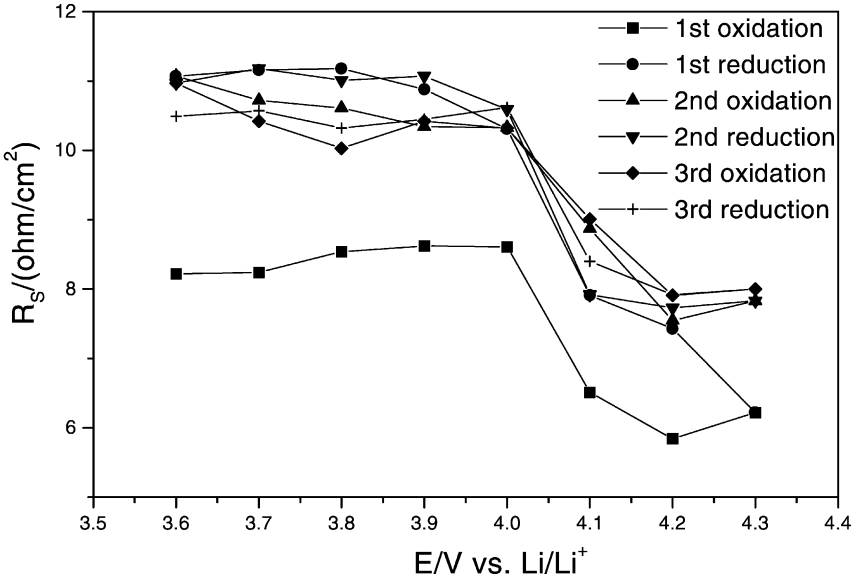

Fig. 8. R_S vs. E deduced from EIS data of $LiMn_2O_4$ film electrode at different potential and cycle number, as indicated.

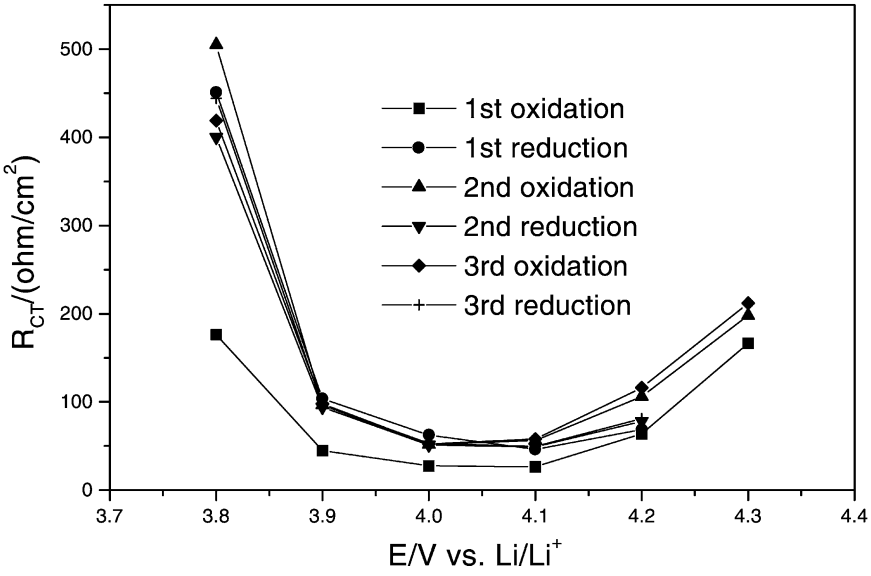

Fig. 9. R_{CT} vs. E deduced from EIS data of $LiMn_2O_4$ film electrode at different potential and cycle number, as indicated.

chronoamperometry [30]. Potential steps of 10 mV were applied to the $LiMn_2O_4$ film electrode through the potential domains of interest (i.e. between 3.9 and 4.3 V versus Li/Li^+). A long time period was used ($t \gg h^2/\pi D$) which corresponds to the finite diffusion case, in which a linear diffusion of Li^+ ions takes place in the bulk of the film with an apparent chemical diffusion coefficient (D). The current response within this time period can be expressed by following equation [31]:

$$\ln i = \ln\left(\frac{2nFAD\Delta C}{h}\right) - \frac{\pi^2 D}{4h^2}t \quad (1)$$

where h is the thickness of the film, A the surface area of the film, ΔC the variation of lithium concentration in the film during the potential step. ΔC can be obtained from the charge injected into the film until the current declined to nearly zero. According to this equation, D can be calculated in two different ways: (i) from the linear slope of ln i versus t; (ii) from the intercept of ln i versus t. The former does not require the value of ΔC, a main advantage because the precise measurement of ΔC is often troublesome due to background currents such as double layer charging current.

Li^+ ion diffusion coefficients between 3.9 and 4.3 V versus Li/Li^+ are presented in Fig. 10. From comparison with the CV curve in Fig. 4, it is confirmed that the plot of log D shows a minimum which correlates with the current peaks in the CV. This observation has also been reported by other workers [32,33] and can be explained by the more

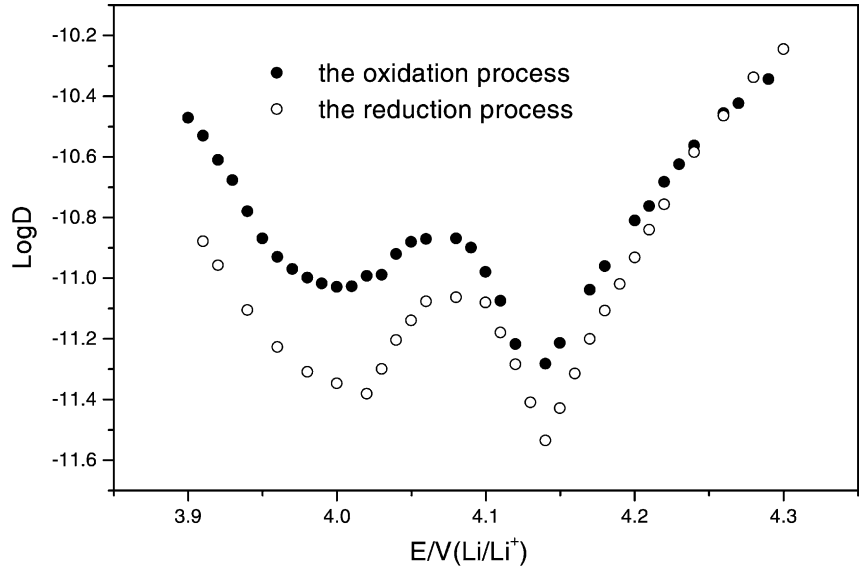

Fig. 10. Dependence of apparent chemical diffusion coefficient (D) on electrode potential where potential step is applied. Width of potential step is 10 mV.

repulsive interaction between the intercalated lithium ions at the CV peak potential. Diffusion coefficients at potentials below 4.15 V are higher in the oxidation process than in the reduction process. At potentials above 4.15 V, however, both the oxidation and the reduction diffusion coefficients are same. This can be assigned to the formation of a surface film at higher potentials. The absence and presence of a surface film is responsible for the difference in the diffusion coefficient at low potential in the oxidation and the reduction process. The lower diffusion coefficient in the reduction process is due to the presence of the surface film which hinders the diffusion of Li^+ ions. The similarity in diffusion at high potentials, however, could be due to the presence of a surface film in each of these the two processes.

4. Conclusions

A $LiMn_2O_4$ film has been prepared using the ESD technique at 400 °C. The XRD pattern demonstrates a well-defined spinel, *Fd*3*m* structure. Electrochemical investigations (CV, EQCM, EIS) of the prepared $LiMn_2O_4$ film confirm dissolution of a Li_2CO_3 layer and formation of new surface film in a $LiCiO_4 + EC + DEC$ electrolyte. The mass of the surface film can be calculated from the resonant frequency curve and is 1.2% of the entire $LiMn_2O_4$ film. It is concluded that abnormal behavior during the first oxidation cycle, which is observed with all the investigative techniques is used in this study, is due to the formation of a new surface film. The latter changes the charge-transfer and surface resistance during the electrochemical processes.

Acknowledgements

One of the authors, Dong Shu, thanks BK21 for the award of a postdoctoral fellowship. The authors thank Dr. Gopu Kumar for help in preparation of manuscript.

References

[1] T. Nagaura, K. Tazawa, Prog. Batt. Solar Cells 9 (1990) 20.
[2] H. Huang, C.A. Vincent, P.G. Bruce, J. Electrochem. Soc. 146 (2) (1999) 481–485.
[3] A. Du Pasquier, A. Blyr, P. Courjal, D. Larcher, G. Amatucci, B. Gerand, J.-M. Tarascon, J. Eletrochem. Soc. 146 (2) (1999) 428–436.
[4] D. Aurbach, K. Gamolsky, B. Markovsky, G. Salitra, Y. Gofer, U. Heider, R. Oesten, M. Schmidt, J. Electrochem. Soc. 147 (4) (2000) 1322–1331.
[5] D.A. Buttry, M.D. Ward, Chem. Rev. 92 (1992) 1355.
[6] D. Aurbach, A. Zaban, J. Electroanal. Chem. 393 (1995) 43–53.
[7] D. Aurbach, A. Zaban, J. Electrochem. Soc. 142 (7) (1995) L108.
[8] H.K. Park, W.H. Smyrl, M.D. Ward, J. Electrochem. Soc. 142 (4) (1995) 1068.
[9] S. Koike, T. Fujieda, R. Sakai, S. Higuchi, J. Power Sources 81–82 (1999) 581–584.
[10] O. Bohnke, B. Vuillemin, C. Gabrielli, Electrochim. Acta 40 (17) (1995) 2755–2764.
[11] D.J. Kim, S.-I.I. Pyun, Y.-M. Choi, Solid State lonics 109 (1998) 81–87.
[12] Y. Yang, D. Shu, H. Yu, X. Xia, Z.G. Lin, J. Power Sources 65 (1997) 227.
[13] T. Uchiyama, M. Nishizawa, T. Itoh, I. Uchida, J. Electrochem. Soc. 147 (6) (2000) 2057–2060.
[14] Y.-M. Choi, S.-I. Shin, H.-C. Shin, Metal Mater. 4 (2) (1998) 193–201.
[15] M. Morita, T. Ichimura, M. Ishikawa, Y. Matsuda, J. Power Sources 68 (1997) 253–257.
[16] M.-R. Lim, W.-I. Cho, K.-B. Kim, J. Power Sources 92 (2001) 168.
[17] C. Chen, E.M. Kelder, J. Schoonman, J. Electrochem. Soc. 144 (1997) L289.
[18] C.H. Chen, E.M. Kelder, M.J.G. Jak, J. Schoonman, Solid State lonics 86–88 (1996) 1301–1306.
[19] C. Chen, E.M. Kelder, P.J.J.M. Van der Put, J. Schoonman, J. Mater. Chem. 6 (5) (1996) 765–771.
[20] A.A. van Zomeren, E.M. Kelder, J.C.M. Marunissen, J. Schoonman, J. Aerosol Sci. 25 (1994) 1229.
[21] D. Zhang, B.N. Popov, R.E. White, J. Power Sources 76 (1998) 81.
[22] J.C. Hunter, J. Solid State Chem. 39 (1981) 142.
[23] J.M. Tarascon, E. Wang, F.K. Shokoohi, J. Electrochem. Soc. 138 (1991) 2859.
[24] M. Nishizawa, T. Uchiyama, T. Itoh, T. Abe, I. Uchida, Langmuir 15 (1999) 4949–4951.
[25] K.Y. Chung, K.-B. Kim, J. Electrochem. Soc. 149 (1) (2002) A79–A85.
[26] Y. Xia, M. Yoshio, J. Electrochem. Soc. 143 (1996) 825.
[27] D. Aurbach, M.D. Levi, K. Gamulski, B. Markovsky, J. Salitra, E. Levi, U. Heider, L. Heider, R. Oesten, J. Power Sources 81–82 (1999) 472–479.
[28] G.X. Wang, D.H. Bradhurst, H.K. Liu, S.X. Dou, Solid State Ionics 120 (1999) 95–101.
[29] M. Nishizawa, T. Ise, H. Koshika, T. Itoh, I. Uchida, Chem. Mater. 12 (2000) 1367.
[30] H. Sato, D. Takahashi, T. Nishina, I. Uchida, J. Power Sources 68 (1997) 540.
[31] C. John Wen, B.A. Boukamp, J. Electrochem. Soc. l2 (1979) 2258.
[32] Y. Yang, D. Shu, J.K. You, Z.J. Lin, J. Power Sources 81–82 (1999) 637.
[33] J. Barker, R. Pynenburg, R. Koksbang, J. Power Sources 52 (1994) 185.